AAAS
Energy Material Advances
Volume 2021, Article ID 1519569, 15 pages
https://doi.org/10.34133/2021/1519569

Energy Material Advances
A SCIENCE PARTNER JOURNAL

Review Article

Porous Mixed Ionic Electronic Conductor Interlayers for Solid-State Batteries

So Yeon Kim and Ju Li

Department of Materials Science and Engineering and Department of Nuclear Science and Engineering, Massachusetts Institute of Technology, Cambridge, MA 02139, USA

Correspondence should be addressed to Ju Li; liju@mit.edu

Received 11 December 2020; Accepted 4 February 2021; Published 29 March 2021

Rechargeable solid-state batteries (SSBs) have emerged as the next-generation energy storage device based on lowered fire hazard and the potential of realizing advanced battery chemistries, such as alkali metal anodes. However, ceramic solid electrolytes (SEs) generally have limited capability in relieving mechanical stress and are not chemically stable against body-centered cubic alkali metals or their alloys with minor solute elements (β-phase). Swelling-then-retreating of β-phase often causes instabilities such as SE fracture and corrosion as well as the loss of electronic/ionic contact, which leads to high charge-transfer resistance, short-circuiting, etc. These challenges have called for the cooperation from other classes of materials and novel nanocomposite architectures in relieving stress and preserving essential contacts while minimizing detrimental disruptions. In this review, we summarize recent progress in addressing these issues by incorporating other classes of materials such as mixed ion-electron conductor (MIEC) porous interlayers and ion-electron insulator (IEI) binders, in addition to SE and metals (e.g., β-phase and current collectors) that are the traditional SSB components. In particular, we focus on providing theoretical interpretations on how open nanoporous MIEC interlayers manipulate β-phase deposition and stripping behavior and thereby suppress such instabilities, referring to the fundamental thermodynamics and kinetics governing the nucleation and growth of the β-phase. The review concludes by describing avenues for the future design of porous MIEC interlayers for SSBs.

1. Introduction

Remarkable breakthroughs in liquid electrolyte- (LE-) based rechargeable Li-ion batteries (LIB) have enabled modern portable electronics and electric vehicles (EVs). Such applications, however, now call for solid-state batteries (SSBs) due to safety concerns and the demand for higher energy density [1, 2]. In this respect, rechargeable alkali metal SSBs with ceramic solid electrolytes (SEs) are promising alternatives, but they have yet to achieve sufficient cycling stability [2]. This review thus is aimed at critically examining the need for SEs and other types of materials in developing safe rechargeable batteries with both high energy density and long-term stability.

With the mass marketing of portable electronics and EVs, the shortcomings of LE-based batteries became more apparent [1]. First, organic LE-based batteries have significant fire and explosion risks due to the high vapor pressure and combustibility of organic liquids when mixed with oxygen gas [3]. They usually have metal oxides with high oxygen content on the cathode and thermally unstable solid electrolyte interphase (SEI) on both electrodes, which is produced by organic LEs reacting with the electrodes. When these batteries are subjected to abuse by faulty operation or traffic accidents, severe thermal runaways can occur, triggered by the liquid's high volatility (equilibrium vapor pressure) and fueled by the cathode's oxygen inventory and SEI decomposition [4]. Second, aqueous LEs, while not as dangerous, traditionally have lower energy density because of a narrower electrochemical stability window $[U_{\text{lower}}, U_{\text{upper}}]$ where U is the absolute electronic potential [5] that is related thermodynamically to a charge-neutral Li-atom's chemical potential embedded in either electrode, beyond which an electrolyte is reduced or oxidized. Third, by dissolving a variety of unwanted stray ions from cathodes (e.g., Mn^{2+} in Li-ion batteries (LIBs) [6] or polysulfides in Li-S batteries [7]) and

conducting them and their solvation shells via vehicular diffusion, LEs often enable cathode-anode shuttling and parasitic reactions that reduce the cycle life and shelf life of batteries.

In contrast, SEs have clear advantages in terms of safety and charge-carrier-transport characteristics. First, most ceramic SEs are less prone to catching fire since they have low vapor pressure and are less flammable than organic LEs [2, 8]. Moreover, most of them can enable advanced battery chemistries that would offer higher energy density by forbidding unwanted ions to pass through them [1]. The total bulk electrical conductivity of any material can be partitioned into transference numbers for various charge carriers such as electrons, a primary cation (e.g., Li^+ for LIBs and Na^+ for sodium-ion batteries), and other ions: $1 = t_{electron} + t_{Li+} + t_{other\ ions}$. In electrolytes, which are electronic insulators, $t_{electron}$ is essentially zero, and ions partition the bulk electrical conductivity. While LEs often have t_{Li+} less than 0.5 due to vehicular diffusions of all free ions with their solvation shells, t_{Li+} of most inorganic SEs is very close to 1 at service temperature [2], and hence, the flow of ions other than Li^+ is strongly *forbidden* in SEs due to the exchange mechanism of diffusion in SEs. This $t_{Li+} = 1$ solves the cathode-anode shuttling and parasitic reaction problem generically, opening up more possible chemistries (like high-energy-density Mn-rich or sulfur cathodes) and a higher temperature range for stable batteries. Furthermore, there is a strong expectation that SEs may enable the use of high-energy-density alkali metal anodes, which can realize longer mileage of EVs [1, 9, 10]. This expectation arose from the SE's relatively high elastic modulus, which was believed to hinder dendritic penetration of β-phase [11], as β-phase tends to be elastically quite soft. It later turned out that high elastic modulus alone cannot combat the dendrite problem when inorganic SEs have preexisting flaws [12], so decent fracture toughness is also required for the SE. Nonetheless, this expectation had motivated intensive research on rechargeable alkali metal SSBs in conjunction with the aforementioned two main advantages of ceramic SEs over LEs (thermal stability, and $t_{Li+} = 1$).

Inspired by these advantages, significant efforts had been dedicated to enhancing the bulk ionic conductivities of SEs as a first step [13–15]. However, now that several SEs [13] have exhibited a bulk ionic conductivity comparable to or even higher than those of the LEs, other properties of SEs have become major bottlenecks. For example, in rechargeable alkali metal SSBs using oxide SEs such as garnet $Li_7La_3Zr_2O_{12}$ (LLZO) or sulfide SEs such as $Li_{10}GeP_2S_{12}$ (LGPS) and argyrodites Li_6PS_5X (X = Cl, Br, I), the electrochemical stability window $[U_{lower}, U_{upper}]$ of SEs, their thermochemical and mechanical stabilities (e.g., toughness), and interfacial wetting with alkali metal phases constitute the main challenges. In this review, the alkali metal-dominated phases of interest include not only metallic Li (Li_{BCC}) and Na (Na_{BCC}) but also their alloys in the body-centered cubic (BCC) structure. These random-solid-solution phases are simply denoted as the "β-phase" in this paper.

The main issues with rechargeable, "β-phase pumping" SSBs all originate from the repetitive swelling-then-retreating of the mechanically stressful and highly corrosive β-phase (e.g., Li_{BCC} or Na_{BCC}). The total volume of the β-phase on the anode side needs to swell and shrink throughout the operation of a rechargeable metal battery. Every 1 mAh cm^{-2} of reversible areal capacity in the Li metal battery requires plating and stripping of an approximately 5 μm thick Li_{BCC} phase, assuming that the Li_{BCC} is fully dense. As SEs lack fluidity (unlike the LEs), this dynamic volume change and the resultant cyclic stress often cause loss of physical contact at the SE/β-phase interface, where it is crucial for the ions and electrons to meet to carry out the anode-side half-cell reactions. Also, many SEs that have high bulk ionic conductivities (e.g., LLZO, LGPS, or Li_6PS_5X) are actually thermodynamically unstable against the Li_{BCC} phase [16–18], as can be seen in Figure 1. They thus undergo corrosive reactions, often generating reaction products that have either Li^+ conductivity lower than the SE or nonzero $t_{electron}$. The former case degrades essential ionic contact, leading to increasing half-cell charge-transfer resistance (R_{ct}) between the SE and the active material, in battery diagnostics such as electrochemical impedance spectroscopy. The latter creates unwanted electron-conducting paths, which can cause continued side reactions electrochemically and eventual short-circuiting. In addition, when stress and corrosion attacks on SEs are combined, they can synergistically work to disrupt essential contacts or create unwanted contacts, sometimes even resulting in SE fracture. The design strategies for "3D" anodes have thus been of great interest, with an emphasis on manipulating the microscopic β-phase deposition and stripping behavior through controlling its nucleation and growth kinetics, that share many common features with classical physical metallurgy examples.

In this review, we begin by summarizing the mechanical-electrochemical origin of the aforementioned instabilities at the SE/β-phase interface. We then examine 3D open porous architectures constructed with different types of materials and discuss possible roles of phase transformation, wetting, diffusion, and β-phase creep/plasticity in mitigating driving forces of instabilities and thereby maintaining acceptable R_{ct} as well as $t_{electron} = 0$ barrier function of SEs. Moreover, since SEs often need to transmit several MPa of pressure, we also assess the role of stack pressure in SSBs, and whether this pressure is absolutely necessary. The traditional components of anodes for rechargeable alkali metal SSBs require SE and metals (e.g., β-phase, and the Cu current collector, CC). The main thesis of this review is that more material classes are required in certain spatial arrangements to achieve long-term stability of rechargeable alkali metal SSBs. In particular, anodes would need to incorporate two additional classes of materials—a mixed ion-electron conductor (MIEC) and an ion-electron insulator (IEI)—of a certain architecture.

2. Evolution of Instabilities in Alkali Metal SSBs

β-phase often corrodes the surrounding material components in rechargeable alkali metal SSBs. In Figure 2, we show that materials can be generally classified into four quadrants according to whether they conduct free electrons and/or the

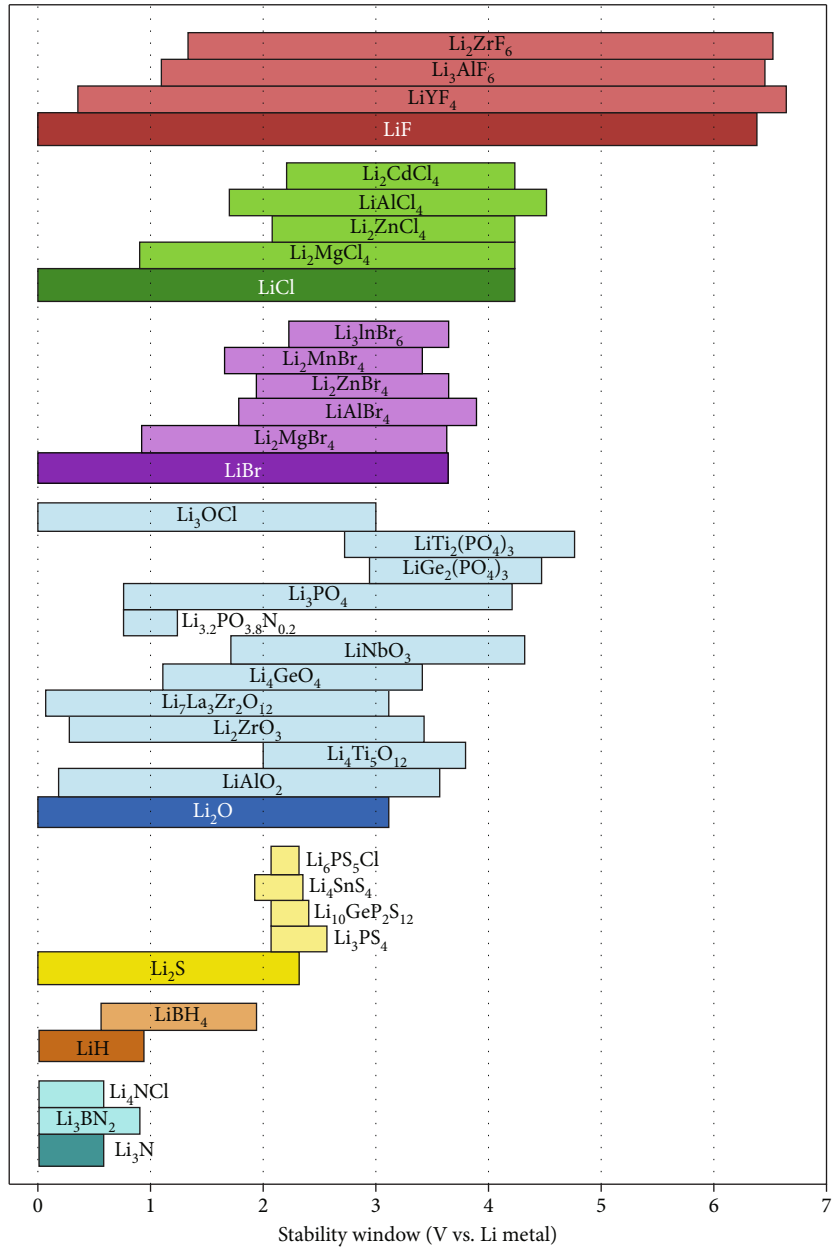

FIGURE 1: Electrochemical stability window $[U_{\text{lower}}, U_{\text{upper}}]$ of various solid electrolytes. Those of the corresponding binary inorganic solids are also provided for comparison. Reproduced from Ref. [18] with permission from American Chemical Society. Further permissions related to this figure should be directed to the American Chemical Society.

primary ion. A metal (M) conducts free electrons but not ions. A solid electrolyte (SE) conducts Li^+ or Na^+ but not free electrons. A mixed ion-electron conductor (MIEC) conducts both Li^+ or Na^+ and electrons (i.e., $t_{\text{ions}} > 0$ and $t_{\text{electron}} > 0$), while an ion-electron insulator (IEI) conducts neither. It is possible to find materials in each of the M, SE, MIEC, and IEI categories which are thermodynamically absolutely stable against Li_{BCC} or Na_{BCC}, but there are many more counter-examples in each category also, because the β-phase is chemically so reactive.

The corrosiveness of β-phase is reflected by the fact that only a small set of compounds among the 200,000+ known crystals in the Inorganic Crystal Structure Database (ICSD) have a direct tie-line to the β-phase on the multi-element phase diagram (e.g., ternary and quaternary phase diagrams shown at https://materialsproject.org). If a solid phase $A_mB_nC_q$ of interest does not have a direct tie-line to Li_{BCC} in a Li-A-B-C phase diagram at the temperature of interest, the mixture of $xA_mB_nC_q$ and yLi_{BCC} by definition would prefer to react and turn into a combination of other intervening phases. That is to say, $A_mB_nC_q$ would have no thermodynamic immunity against β-phase corrosion. If we think of a ternary phase diagram as a "flight map," then only the phases with "direct flight" to the city

	Ion conductor	Ion insulator
Electron conductor	Ion conductor and electron conductor a.k.a. Mixed ion-electron conductors (MIEC) e.g., LiC_6, LiAl, $Li_{22}Si_4$, for Li^+	Ion insulator and electron conductor a.k.a. normal metal (M) e.g., Ni, Stainless steel
Electron insulator	Ion conductor and electron insulator a.k.a. Solid electrolyte (SE) e.g., $Li_7La_3Zr_2O_{12}$, $L_{10}GeP_2S_{12}$	Ion insulator and electron insulator (IEI) e.g., BeO, SrF_2 for Li^+

Figure 2: Four different types of materials classified according to whether they conduct electrons and/or primary ions. Examples of mixed ion-electron conductors (MIEC) and ion-electron insulators (IEI) are provided, taking Li^+ as primary ions.

of β-phase (e.g., tie-line) are stable when spatially put side-by-side with the β-phase. This also means all other phases with minimally more than one transit to reach the β-phase would be thermodynamically unstable against it.

If the SE in a rechargeable SSB is $A_mB_nC_q$ that does not have a direct tie-line to the β-phase, the corrosive $xA_mB_nC_q + yLi_{BCC}$ reaction happens and gives rise to different instabilities depending on the transference numbers of the *reaction products*. First, suppose that the reaction products are either M or MIEC, which have nonzero $t_{electron}$. If not kinetically stopped, the $xA_mB_nC_q + yLi_{BCC}$ reaction will proceed in a self-perpetuating manner during the charging process. This is because $xA_mB_nC_q$ will then have kinetic access to both Li^+ (SE or MIEC) and e^- (M or MIEC), which would combine to produce additional charge-neutral Li atoms under a cathodic current by the following charge-transfer half-cell reaction $Li^+(SE, MIEC) + e^-(M, MIEC) =$ Li atom in the Li_{BCC} phase. As the anode's potential drops below 0 V versus Li upon charging of the full cell to give a driving force for Li_{BCC} deposition to happen, there will be a continuous supply of Li atoms into the $xA_mB_nC_q + yLi_{BCC}$ system at a chemical potential μ_{Li} equal to or lower than that of Li atoms residing in the Li_{BCC} phase. In other words, y will continue to increase, and the $xA_mB_nC_q + yLi_{BCC}$ reaction will keep proceeding forward, further converting SE to more M or MIEC. Such reductive metallization may occur preferentially along the grain boundary (GB) network of SEs and can eventually cause SE failure and short-circuiting, which is often diagnosed as showing near-zero open-circuit voltage in battery full cells.

In contrast, suppose that the reaction products have $t_{electron} = 0$ and have direct tie-line to the β-phase themselves so they are stable side-by-side with β. They may then form a kinetic passivation layer, cutting off the supply of free electrons, which would have otherwise combined with Li^+ to offer Li atoms to the $xA_mB_nC_q + yLi_{BCC}$ system. If this layer is sufficiently compact and adherent, it will stop corrosive reactions kinetically, being the reductive analog of Al_2O_3 on Al in an oxidizing environment [19]. This layer can, however, have much poorer ionic conductivity than the original SE—Li_2O could form, for example—or even become an IEI. Such conversion would cause an increase of R_{ct} in future cycles. Therefore, it is often an "either a drought or a flood" problem when corrosion of original SE occurs. Also, it is usually the case that this passivation layer does not last very long due to the mechanically stressful β-phase.

Next, we address the stressful aspect of the β-phase and the resultant electrochemomechanical instabilities. Stress can be easily generated in the course of β-phase deposition and stripping, as seen in the thermodynamics of the reaction:

$$Li^+(SE \text{ or } MIEC) + e^-(U) = Li \text{ atom in } \beta\text{-phase} \quad (1)$$

where U is the local electronic potential in M or MIEC that feeds the electron to the site of the reaction above. For the right-hand side, there is

$$\mu_{Li}(Li \text{ atom in } \beta\text{-phase}) = \mu_{Li}^{\circ} + k_B T \ln(\gamma_{Li} X_{Li}) + \Omega_{Li} P(\mathbf{x}) \quad (2)$$

to leading order, where μ_{Li}° is the reference chemical potential of Li atom in pure Li_{BCC} in stress-free condition, $\gamma_{Li}X_{Li}$ is the composition-dependent chemical activity, and Ω_{Li} is the partial molar volume of Li atom (~21.6 Å^3) in β-phase. $P(\mathbf{x}) = -\mathrm{Tr}(\boldsymbol{\sigma}(\mathbf{x}))/3$, where $\boldsymbol{\sigma}(\mathbf{x})$ is the position-dependent mechanical stress field. Equating the left- and right-hand side of Equation (1) shows that an increase of the local overpotential by just 0.135 V can cause GPa-level stress inside the β-phase if a thermodynamic equilibrium is to be reached [20].

The insertion volume and generated stress mechanically load up SSBs' solid components, thereby driving fatigue and failure. Some of the *in situ* formed passivation layers may not be able to withstand such stresses and end up being spalled off as electron-insulating debris. This spallation would lead to capacity loss as the active Li would be

consumed to form a new passivation layer, and the debris can also disrupt or block the electron-conducting paths. Moreover, since the stresses with an opposite sign arise during discharging, the solid components of SSBs are subjected to cyclic stresses throughout the operation, which can deteriorate interfacial contact and drive fatigue crack growth. Particularly, β-phase deposition at preexisting flaws on the surface of SEs generates crack-tip stress, which drives crack propagation [12]. As the surface flaws and cracks are favorable nucleation sites [21], this attack generally occurs in a self-reinforcing manner, forming dendrites, and results in SE fracture and short-circuiting.

The pressure in the β-phase can be relaxed by plastic deformation driven by a pressure gradient $\nabla P(\boldsymbol{x})$ and shear stress—it can be shown that there has to be deviatoric shear stress whenever there is a $\nabla P(\boldsymbol{x})$—that allow the atoms in β-phase to either convect or diffuse into adjacent spaces. Such stress relaxation requires either prearranged empty space (reserved porosity) or working against the stack pressure to create the extra space for insertion. If the former route is taken, the convection or diffusion of Li atoms in the β-phase, or at the interface with the β-phase, must be facile enough to cover the distance between where reaction (1) happens and where the reserved porosity is. This process then involves either displacive deformation or diffusion of the metal atoms. In addition, nucleation of the β-phase is also required, and standard metallurgical treatment of the interfacial wetting, heterogeneous nucleation, and Gibbs-Thomson effect induced coarsening/ripening needs to be discussed. Lastly, we note that the reserved pore spaces with vacuum or inert gas can be considered a type of IEI, although typically we take IEI to mean the binder solid phase between SE and MIEC [20].

3. Materials and Architecture

One promising approach adopted to relieve the corrosion and stress attacks from the β-phase on the move is to accommodate it in a 3D MIEC architecture with prereserved porous regions. For instance, Xu et al. [22] introduced a MIEC framework, where a 3D porous garnet structure is covered by a conformal carbon nanotube coating (Figure 3(a)), and achieved stable cycling over a few tens of cycles at a high current density of $\geq$~1 mA cm^{-2}. The garnet conducts Li^+, whereas the carbon nanotube conducts both electrons and Li^+ upon lithiation. Alloy-type MIECs have also been employed. For example, Yang et al. [23] cycled Li-Mg random-solid-solution alloy, which has an appreciable solubility of Li atoms and thus can be considered as a MIEC, and reported stable cycling over a few hundred cycles at a high current density of $\geq$~1 mA cm^{-2}. Furthermore, Zhu et al. [24] utilized a Sn-Ni alloy-coated Cu nanowire network as an anode (Figure 3(b)), where Li-Sn intermetallic compound forms upon lithiation and functions as a MIEC. They demonstrated a notable improvement in rate capability—a doubling of capacity at 5C and a more than five times increase in cycle life at 1C as compared to the Li metal anode—without detrimental corrosion or stress-induced collapse.

MIECs have been chosen as the base materials for the porous interlayer or 3D electrode by virtue of their conduction properties. First, having kinetic access to both Li^+ and electrons, they can provide sites for reaction (1) to occur, and hence curtail Li atom insertion at the SE/β-phase interface; the large surface area of the 3D porous MIEC gives it an advantage. It has thus been expected that 3D MIEC architectures would alleviate spallation at the SE/β-phase interface and the associated capacity loss [26]. Meanwhile, the spallation at the MIEC/β-phase interface has generally been thought to be negligible since the formation of interphase (e.g., passivation layer) itself can be prevented by employing the MIECs that are thermodynamically absolutely stable (not just kinetically passivated) in the range of operating Li potentials [26]. Second, porous MIECs can secure electron-conducting paths even when there exists electron-insulating debris spalled off from the SE/β-phase interface as they conduct electrons in a redundantly percolating fashion. As the rate at which R_{ct} increases upon cycling can be slowed down in 3D porous MIEC-assisted SSBs, better rate capability can be anticipated [22–24].

Based on MIECs' conduction properties and 3D architectures' open porosity, 3D MIEC architectures have been expected to realize pragmatic rechargeable SSBs by accomplishing high energy density, long-term stability, and rate capability simultaneously. That being said, most of the 3D MIEC architectures did not prevent direct contact of β-phase with an SE, leaving the progressive evolution of interfacial instabilities still possible, especially when high stresses are involved. The bulk ionic conductivities of inorganic SEs should be orders of magnitude smaller than the bulk electronic conductivities of many MIECs. Electrons should thus arrive "earlier" at the SE/MIEC interface and "wait" for Li^+ (or Na^+) that travel through the SEs to arrive, thereby potentially creating β-phase at the SE/MIEC interface and engendering undesired stress. Mitigating this concern fundamentally demands a better understanding of the β-phase deposition/stripping kinetics based on the nucleation and growth of metals and alloys, and size dependence of these behaviors. Note that we use the word "mitigate" instead of "eliminate," as β-phase may never be completely eliminated at/near the MIEC/SE interface. However, as long as those β-phases are small in quantity and do not have high mechanical stress, they will not be as aggressive and damaging to the SE.

A mechanistic understanding of how 3D MIEC architectures manage β-phase "pumping" has been provided using a simple structure consisting of aligned open-porous carbon tubules by Chen et al. [20]. Figure 3(c) shows the cross-sectional schematic of the adopted cell configuration on the anode side. The MIEC tubules are colored red. The ends of the tubules are rooted in the SE and the metallic current collector (CC), respectively. CC is typically copper or stainless steel foil. In this cell configuration, the neutralized metallic Li atoms are still produced mostly at the SE/MIEC interface (or SE/Li_{BCC} interface in later stages). The continuous insertion of Li during plating, however, generates high compressive stress at this interface as discussed above. Since the other end of the Li_{BCC} is the free surface with nearly zero

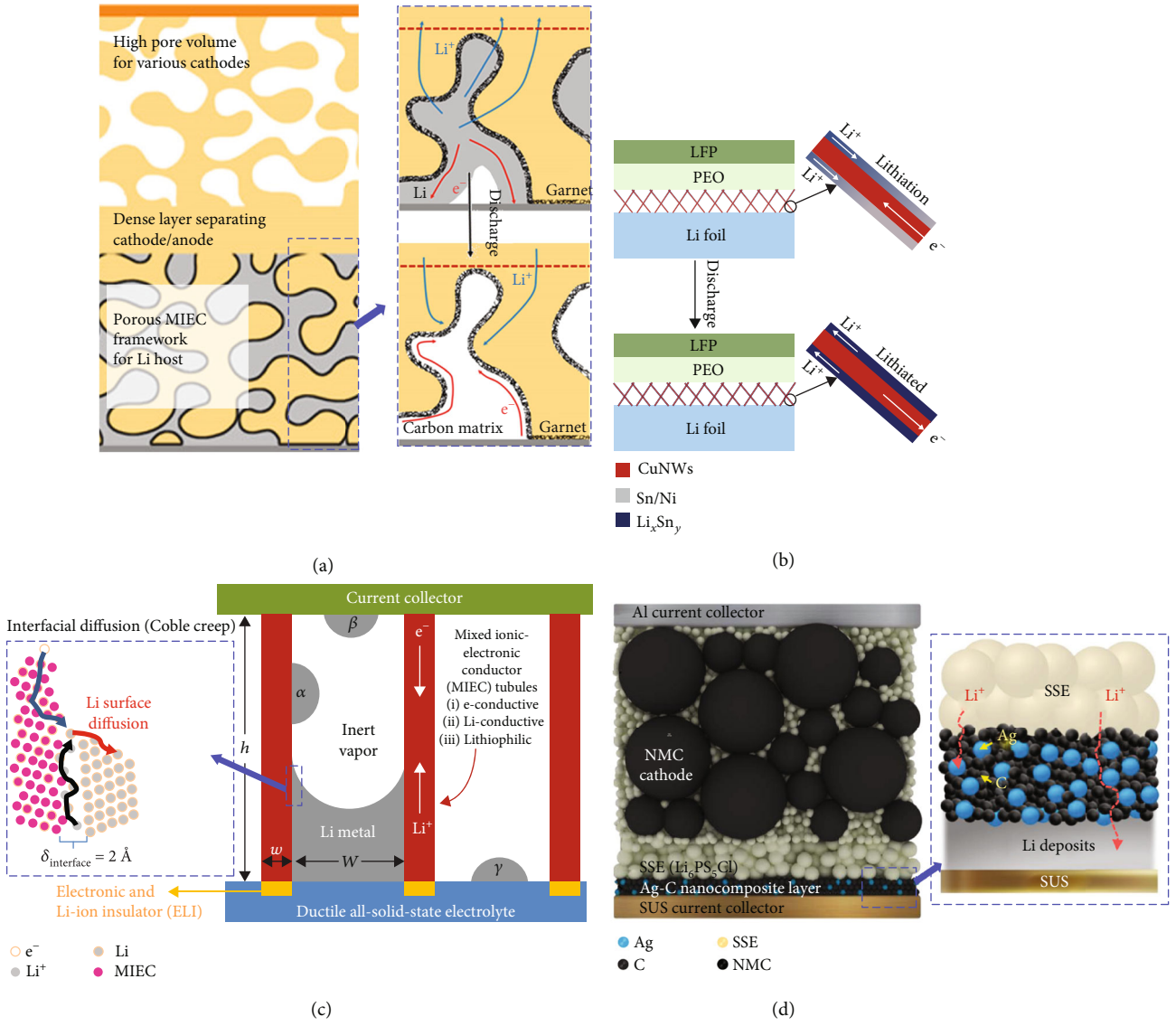

FIGURE 3: Architecture of solid-state batteries with a porous mixed ion-electron conductor (MIEC) interlayer on the anode side. (a) Garnet coated with carbon nanotubes. Adapted with permission from Ref. [22]. Copyright (2018) American Chemical Society. (b) Cu nanowire coated with Sn-Ni alloy. Reprinted with permission from Ref. [24]. Copyright (2019) American Chemical Society. (c) Aligned MIEC tubules. (d) Ag-C nanocomposite. (c) and (d) are adapted from Ref. [20] and Ref. [25], respectively, with permission from Springer Nature.

pressure, the pressure difference and the resultant gradient in the chemical potential of Li_{BCC} develop throughout the tubules [20, 27, 28]. This gradient provides the driving force for the transport of metallic Li from the SE side to the CC side. Moreover, from the aspect of kinetics, it has been pointed out that the low melting point of Li_{BCC} and large interfacial area that the 3D architecture provides would allow Li atoms to diffuse rapidly along the wall or surface of the MIEC [29] (namely, Coble creep), as illustrated in the boxed area of Figure 3(c).

These findings provide important boundary conditions regarding the β-phase deposition. First, they indicate that β-phase can nucleate at or infuse into the interface between the roots of the MIEC and the SE, which is unfavorable from the viewpoint of structural stability. Provided that the MIEC has a good wettability by the β-phase, which is in fact a desirable property to offer appreciable interfacial solubility (i.e., segregation) and diffusion rate, the interface between the SE and the MIEC could also be an attractive site for heterogeneous nucleation of β-phase due to the low nucleation barrier therein. Subsequently, the soft β-phase infused between SE/MIEC can enable interfacial sliding like a lubricant, thereby making the MIEC roots mechanically unstable and facilitating interfacial decohesion upon stripping. Hence, 3D MIEC/SE architecture alone would be electrochemomechanically unstable unless large-scale β-phase invasion into MIEC/SE interface is averted [20, 26]. To circumvent this issue, it is proposed to cover the root with an IEI (colored yellow in Figure 3(c)), which is a class of materials that has not been used for anode construction [20]. The IEI layer is expected to prevent β-phase deposition at the root and function as a mechanical binder [20]. To function properly, an IEI

should be not only insulating to both electrons and ions but also thermodynamically stable against β-phase [20]. It has thus been suggested that IEIs for this use should sit on a direct tie-line with the β-phase in the phase diagram with minimal Li solubility (lithiophobic [30]) and have a large electronic bandgap, like over 4.0 eV [20], to be sufficiently electronically insulating and stopping β-phase nucleation and/or aggression.

Second, if nucleation barriers at different interfaces are properly manipulated, it might be possible to induce β-phase to nucleate elsewhere other than the SE/MIEC interface or coarsen away the β-phase at SE/MIEC interface even if it is nucleated. In this respect, one 3D MIEC architecture worth noting is the Ag-C nanocomposite recently developed by Lee et al. [25], which has been verified to deposit β-phase at the MIEC/CC interface. It was constructed of carbon black powders and Ag nanoparticles with the diameter of ~60 nm. A schematic representation of the cross-section of the cell is provided in Figure 3(d). As the carbon black conducts both Li^+ and electrons, this nanocomposite can be considered as an open-porous MIEC with the inner surfaces decorated with Ag. Interestingly, β-phase with dissolved Ag was formed between the MIEC and the CC as shown in the boxed area of Figure 3(d). The SE/MIEC interface remained largely free of direct contact with β-phase, unlike those in most of the MIEC-based 3D architectures, which establish direct contact with β-phase. Aided by the electrochemical and mechanical stability at the interface, this cell achieved Coulombic efficiency as high as 99.8% when averaged over 1,000 cycles, which is by far the best performance among the reported rechargeable alkali metal SSBs in terms of cycle life and long-term Coulombic efficiency [31, 32].

4. Mechanisms

To understand the mechanism underlying the β-phase deposition at the MIEC/CC interface, the evolution of microstructures upon charging/discharging was investigated with a focus on the room-temperature redistribution of both metallic Li and Ag [25]. Figure 4 shows the schematic of β-phase deposition/stripping through the open-porous MIEC interlayer with metal nanoparticles and microstructure evolution therein (Figure 4(a)) as well as the experimental observations (Figures 4(b) and 4(c)). First, the electron energy loss spectroscopy analyses and selected area diffraction pattern analyses with a transmission electron microscope (Figure 4(b)) revealed that Ag nanoparticles undergo morphological and structural changes during cycling, which suggests the formation of Li-Ag alloys inside the MIEC interlayer. Second, the energy dispersive spectroscopy analyses in a scanning electron microscope (Figure 4(c)) showed that most of the metallic Ag moves to the CC side (instead of the SE side) and forms β-phase there during charging. It goes back to the MIEC interlayer upon discharging; however, Ag that was dissolved in the β-phase remains mostly at the CC side of the MIEC interlayer, making the distribution of Ag inside the MIEC interlayer more and more asymmetric. Lastly, in terms of morphology, Ag nanoparticles in the MIEC layer were found to become fragmented upon cycling, but no instabilities such as pores were observed at the solid-solid interfaces. Based on these experimental findings, we describe next the thermodynamic driving forces that may be responsible for the microstructural evolution as well as the kinetic feasibility of such asymmetry development.

4.1. Li Deposition at MIEC/CC Interface. One of the most important yet puzzling features is that the β-phase layer is formed at the MIEC/CC interface as shown in Figure 4(c) [25]. It is generally thought that the rate-limiting factor in rechargeable SSBs is long-range ion transport in an SE [33, 34]. However, if the long-range transport was the dominant factor, β-phase should have nucleated at the SE/MIEC interface instead of the MIEC/CC interface, since the SE's ionic conductivity should be several orders of magnitude smaller than the MIEC's electronic conductivity. Such an issue was also revealed from a careful intrinsic rate capability study of rechargeable Na-ion SSBs [35]. Their rate performance was greatly improved when the R_{ct} was lowered, while the change of the SE's bulk ionic conductivity in the range of 0.48–0.12 mS cm^{-1} caused no difference. These observations indicate that the charge transfer reactions on the anode side can be governed by short-range, reaction-limited kinetics (phase nucleation barriers, interfacial wetting, Butler-Volmer electron transfer rate, etc.), given that SE's bulk ionic conductivity is already in an acceptably high range.

Indeed, the open porous MIEC interlayer architecture with Ag creates an environment in which short-range R_{ct}, not long-range transport, can manipulate Li_{BCC} nucleation sites. First, the argyrodite-based SE has a bulk ionic conductivity greater than 1 mS cm^{-1} [25], which satisfies the minimum requirement on the conductivity to allow other factors to be a determinant. Second, the MIEC interlayer's porosity can decrease R_{ct}. R_{ct} is the only term that physically should scale with the true contact area in most equivalent-circuit models of the battery. As the porosity provides a large surface or interfacial contact area, it would help lower R_{ct}. Finally, Ag nanoparticles can reduce the β-phase nucleation barrier. In rechargeable alkali metal SSBs, charge transfer reactions involve β-phase nucleation, in which the energy barrier depends on the interfacial wetting [21]; the greater the wettability (i.e., the smaller the wetting angle), the lower the barrier. The wettability of Ag nanoparticles by Li_{BCC} is better than that of the MIEC by virtue of their metallic character and Ag's solubility in Li_{BCC} (~1 at.% at room temperature [36, 37]). They can thus lower the nucleation barrier and R_{ct}. The recent finding that the overpotential required for β-phase nucleation on substrates with definite solubility in Li_{BCC} (e.g., Au, Ag, Mg, Al, and Pt) is nearly zero provides a proof of principle for this effect [38] of lowering the β-phase nucleation barrier. Hence, R_{ct} might have motivated Li_{BCC} to nucleate first at the inner surfaces of the MIEC interlayer.

That being said, R_{ct} alone cannot explain the β-phase location after first charging. Following the Li_{BCC} nucleation inside the MIEC, coarsening would occur due to the Gibbs-Thomson effect [21]; different surface curvatures of the deposits raise the chemical potential of the components in each deposit to different extents, thereby making them favor

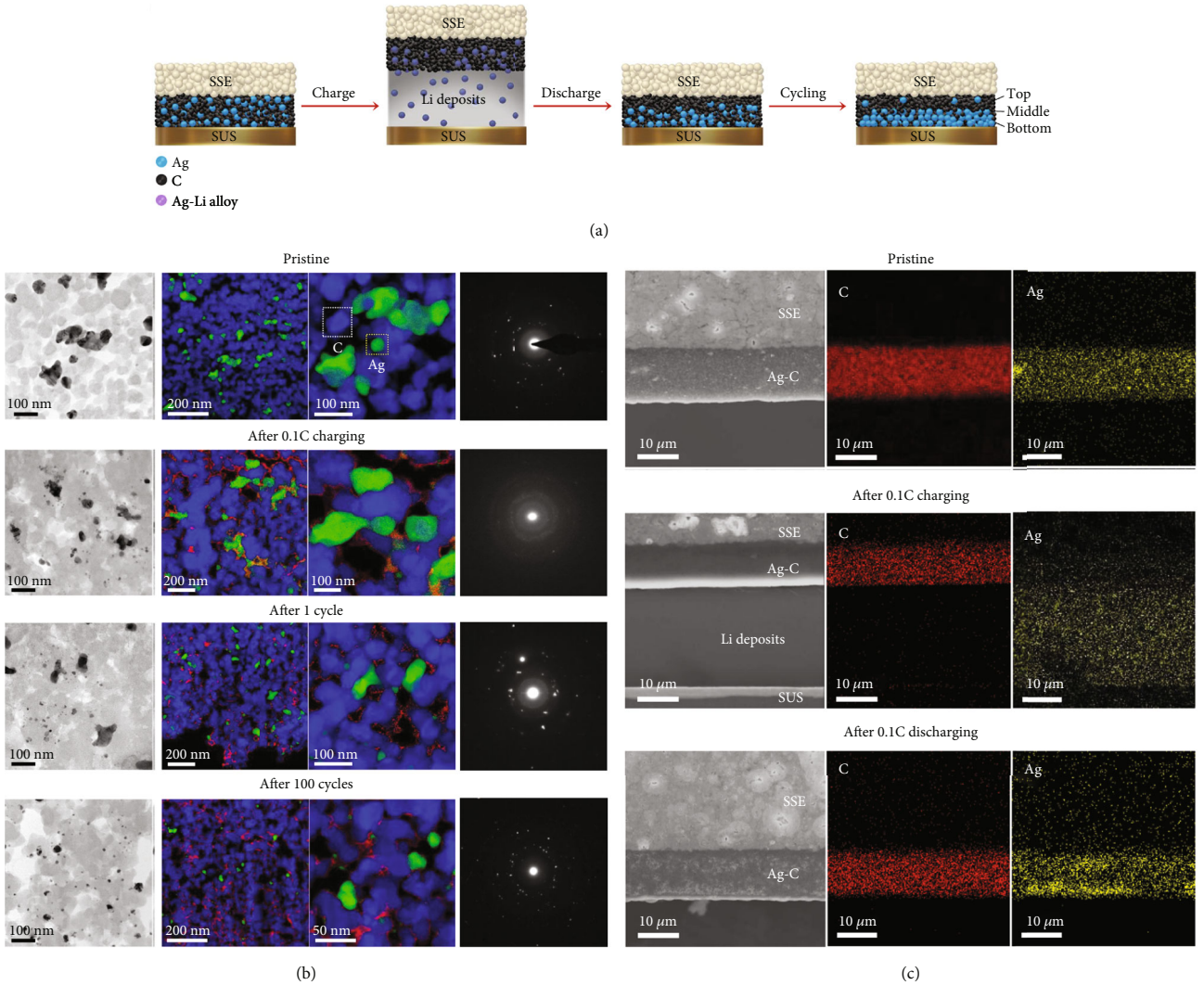

Figure 4: Microstructural evolution during β-phase deposition and stripping through the open-porous MIEC interlayer. (a) Schematic representation of the movement of different metallic elements during charging and discharging processes. (b) Cross-sectional TEM, corresponding EDS images, and the selected area diffraction patterns of Ag nanoparticles in the MIEC interlayer at four different stages: pristine, after 0.1C charging, after 1 cycle, and after 100 cycles. (c) Cross-sectional SEM and corresponding EDS images for the MIEC interlayer at three different stages: pristine, after 0.1C charging, and after 0.1C discharging. Adapted from Ref. [25] with permission from Springer Nature.

some deposits over the others. As the curvature term is inversely proportional to the radius of the deposits [21], this term is essentially zero for a flat surface. Hence, the deposits would eventually reside at either the SE/MIEC interface or the MIEC/CC interface that are flatter rather than on the inner surface of the MIEC, which is wavier. The MIEC/CC interface, however, does not have an advantage over the SE/MIEC interface in terms of the transport distance. It is thus likely that other factors such as interface chemistry play some role. One possible scenario is that metallic Li or Ag atoms near the SE/MIEC interface react with the SEs and form IEIs (e.g., Li_2S or Ag_2S) during a warm-isostatic-pressing process, which is conducted to improve the contact at the SE/MIEC interface. The presence of IEIs may provide a stronger adhesive force while lowering electronic conductivity, thereby making the interface more Li-repellant.

On the other hand, β-phase deposition at the MIEC/CC interface would be achieved more easily in the subsequent cycles owing to the extensive transport of metallic Ag to the CC side during the first cycle. The current collector (made of stainless steel or copper) may have a better wetting angle with Ag and is more "*argenphilic*" (silver is *argentum* in Latin and *argunas* in Sanskrit) than the SE. As shown in Figure 4(c), metallic Ag in the MIEC interlayer moves to the CC side during charging, but it does not restore its uniform distribution upon discharging. Instead, it shows a higher concentration near the MIEC/CC interface. Considering that metallic Ag lowers R_{ct}, this movement would result in a further reduction of R_{ct} at this interface, and thus, metallic Li would favor the MIEC/CC interface in the later cycles. This conjecture is also in good accordance with the relatively low R_{ct} value (~5 Ω cm^2 at 60°C) provided in the paper [25],

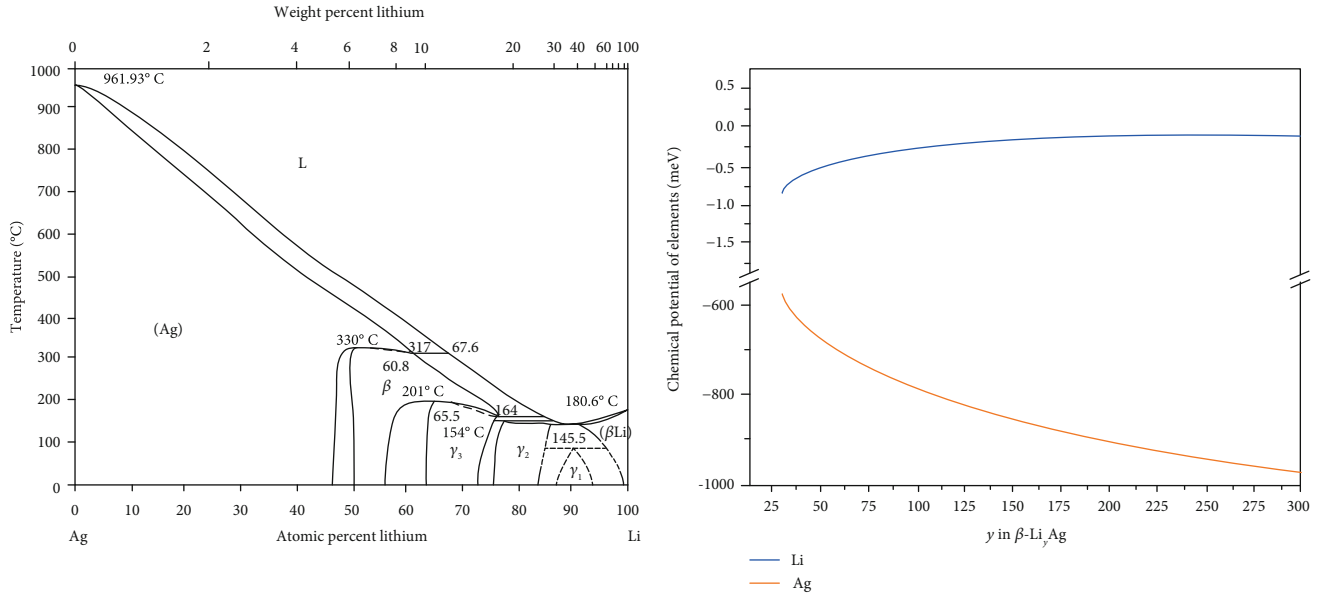

FIGURE 5: Thermodynamics of the Li-Ag system. (a) Phase diagram of the Li-Ag system. (b) Chemical potentials of metallic Li and Ag in the β-Li$_y$Ag phase as a function of y at room temperature in a large y regime. (a) is reproduced from Ref. [37]. Copyright (2010) Elsevier Masson SAS. All rights reserved.

which was measured via the electrochemical impedance spectroscopy after charging.

4.2. Ag Transport at Room Temperature. The next step is to ascertain why and how metallic Ag moves at room temperature (RT). To determine the thermodynamic driving force for the diffusion of metallic Ag, the phase where Ag atoms reside should first be identified. The maximum Ag content is limited by the amount of Ag employed in cell preparation, which is 8–16 mg Ah^{-1}. Since 1 Ah corresponds to 259 mg of Li, the maximum content of Ag in Li$_{BCC}$ at the MIEC/CC interface is approximately 0.4 at.%. The Li$_{BCC}$ with Ag atoms would thus be in the solid-solution β-phase regime (β-Li$_y$Ag) shown in the Li-Ag phase diagram [36, 37] (Figure 5(a)), where y is greater than 249.

The driving force for Ag diffusion is expected to arise from the decrease in total chemical potential change upon alloying/dealloying of Ag into β-Li$_y$Ag. The chemical potentials of metallic Li and Ag in the β-Li$_y$Ag phase regime have not been measured experimentally. They can, however, be estimated via Raoult's law and Henry's law in solution thermodynamics. Raoult's law states that the solvent of a nonideal solution approaches ideal behavior when its concentration approaches unity [39]. When the reference state is Raoultian, it is expressed in a mathematical form as follows: $(da_1/dX_1)_{X_1 \to 1} = 1$, where a_1 and X_1 are the activity and concentration of the solvent (numbered 1), respectively. On the other hand, Henry's law states that the activity of the solute is proportional to its concentration when it is very dilute [39]. This statement implies that the activity coefficient of the solute (numbered 2) in the very dilute binary solution (γ_2^{∞}) has a nonzero finite value. Therefore, assuming that the β-Li$_y$Ag is dilute enough for Raoult's law and Henry's law to work and that the chemical potentials for Raoultian reference states are 0, the chemical potentials of metallic Li and Ag in the β-Li$_y$Ag phase (μ_{Li}^{β} and μ_{Ag}^{β}) are estimated as follows:

$$\mu_{Li}^{\beta} \approx k_B T \ln\left(1 - X_{Ag}\right) \approx -X_{Ag} k_B T, \tag{3}$$

$$\mu_{Ag}^{\beta} \approx k_B T \ln \gamma_{Ag}^{\infty} X_{Ag}, \tag{4}$$

where k_B is the Boltzmann's constant, T is the temperature, and X_{Ag} is the Ag concentration.

The estimated μ_{Li}^{β} and μ_{Ag}^{β} at RT are plotted against y in Figure 5(b). The γ_{Ag}^{∞} value was calculated via the CALculation of PHAse Diagrams (CALPHAD) method; the details are provided in Supplementary Materials (available here). Figure 5(b) shows that μ_{Ag}^{β} decreases more rapidly than the rate at which μ_{Li}^{β} increases upon dissolving metallic Ag into β-Li$_y$Ag. This trend means that Ag atoms in the β-Li$_y$Ag become much more stable as more and more metallic Ag enters the β-Li$_y$Ag, while Li atoms in the β-Li$_y$Ag become only slightly less stable. When the amount of each element is considered, the change in total chemical potential of Ag ($\sim X_{Ag}\Delta\mu_{Ag}^{\beta}$) is likely to be at least two times larger than that of Li ($\sim X_{Li}\Delta\mu_{Li}^{\beta}$). This change would establish a driving force for rapid inward diffusion of metallic Ag into the β-Li$_y$Ag phase along the porous MIEC and the grain boundaries.

The subsequent question to address is whether the long-range transport of metallic Ag at RT is kinetically

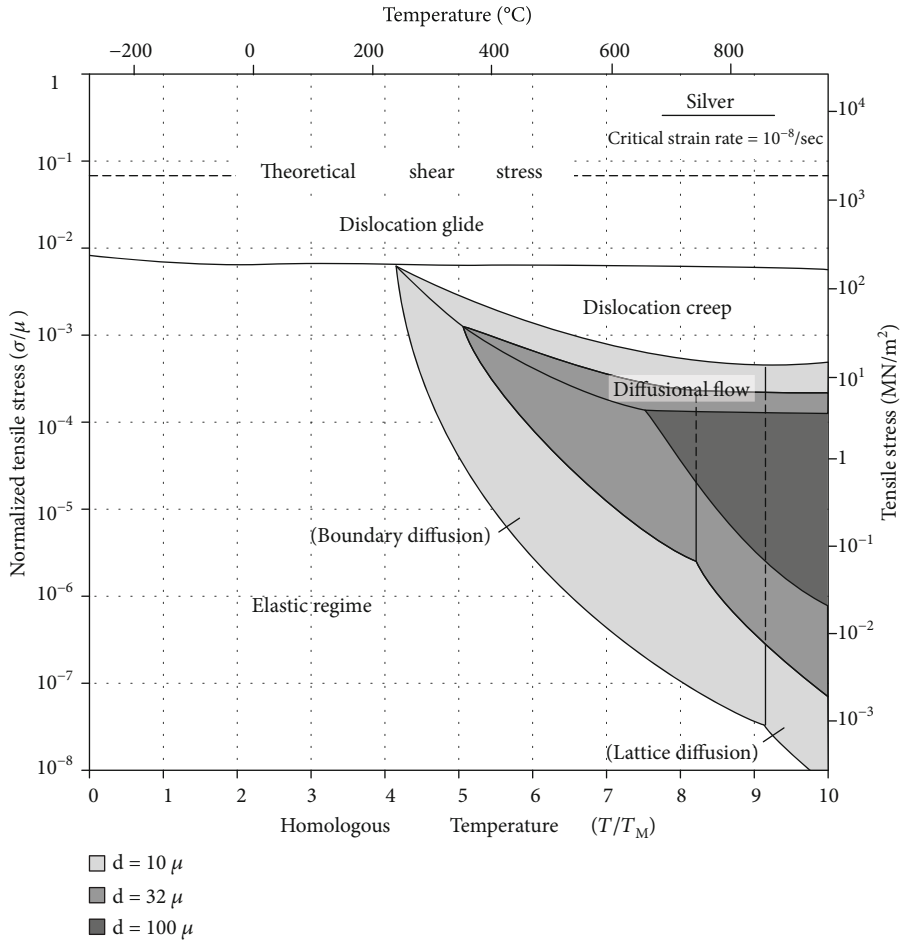

FIGURE 6: Deformation mechanism map for pure Ag for a critical strain rate of 10^{-8} s^{-1}. The diffusional flow fields expand or contract upon changing the grain size (d). Adapted from Ref. [29] with permission from Elsevier.

feasible. Chen et al. [20] have shown that Li_{BCC}, which has a low melting point (~453 K), can advance and retract within the 3D open-porous MIEC at RT via interfacial diffusion, at a timescale acceptable for a battery to function. The pure Ag in the FCC phase, however, has a relatively high melting point (~1235 K). Figure 6 shows the deformation mechanism map of Ag_{FCC} [29]. Metals can deform via either a displacive mechanism (e.g., dislocation glide) or a diffusional mechanism. As the former is viable only when high stress exists (a thresholding, nonlinear, behavior), the latter governs the deformation in the low-stress regime, which is *what we want* for pumping the β-phase. Since the stress greater than 5 MPa is expected to severely degrade the SE life [40], we can assume that the stress in this rechargeable SSB was less than 5 MPa. When the shear modulus of Ag (30 GPa) and its homologous temperature ($T/T_M \sim 0.24$) are considered, Ag_{FCC} would be in the elastic regime of the map.

However, Ag transport may yet be carried out by the interfacial diffusion owing to the nanolevel microstructural length scales of the MIEC interlayer. The $\dot{\varepsilon}$ that can be achieved via interfacial diffusion is inversely proportional to grain size (d) to the power of 3 as seen from the equation [29]:

$$\dot{\varepsilon} \cong \left(\frac{C\sigma}{d^3}\right) e^{-Q/k_B T}, \tag{5}$$

where C is a constant, σ is the applied stress, Q is the activation energy, k_B is the Boltzmann's constant, and T is the temperature. When the diameter of Ag nanoparticles (60 nm) is considered, the $\dot{\varepsilon}$ would be on the order of 10^{-8} s^{-1}. This is an appreciable rate, which pure metals with sub-mm grains in a low-pressure regime can achieve at temperatures near their melting points. Indeed, it has been demonstrated both experimentally and computationally that surface diffusion on sub 10 nm crystalline Ag particles is fast enough to mediate liquid-like pseudoelasticity [41] at room temperature. Its transport at RT can thus be regarded as feasible if nanostructuring of the MIEC interlayer is carried out.

Moreover, the low liquidus/solidus temperatures in the β-Li_yAg phase regime and grain boundary premelting phenomena may also facilitate the interfacial diffusion of both

Ag and Li atoms. The atomic structure of surfaces, grain boundaries, and other interfaces tend to become increasingly disordered when the temperature approaches the bulk melting point, T_M [42]. In the case of alloys, the solidus temperature is considered instead of T_M [42], and that of the β-Li_yAg phase is lower than the T_M of Li_{BCC}. Given that Ag atoms segregate to the grain boundaries, the effective composition along diffusion paths would be near the eutectic point, which has the lowest melting temperature. This means that it might be even easier to diffuse Ag atoms at this composition along MIEC surfaces/interfaces than Li atoms in pure Li_{BCC}. In addition, the atomic size mismatch and the electronegativity difference between Ag and Li may intensify the disordering [36, 42–44] and result in the early premelting. In fact, Ag is known for anomalous diffusion ability in various research fields such as electronic materials [45] and nuclear materials [46]; this ability may have to do with the fact that Ag forms eutectic points with many other metallic elements, making the resultant alloys prone to premelting and interfacial segregation on MIEC surface. This, combined with the possible "argenphilicity" of the current collector versus the "argenphobicity" of the SE side, may explain the gradual asymmetry of the Ag distribution as the MIEC interlayer pumps Li up and down many times with battery cycling [25].

4.3. Suppression of Morphological Instability at MIEC/β-Phase Interface. Another promising feature to note in Ref. [25] is that the MIEC/β-phase interface is free of microscale pores even after 100 cycles at 0.5C, which corresponds to a high current density of 3.4 mA cm^{-2}. Rechargeable Li metal SSBs have often suffered from a pore formation problem due to the slow diffusion kinetics [23, 47, 48]. Upon applying anodic current, a neutral Li atom in the β-phase loses one electron and becomes Li^+, which then diffuses via the MIEC + SE to the cathode, leaving a vacancy. The difference in the vacancy concentration then drives the diffusion of Li atoms to the interface where the charge-transfer reaction takes place [47]. If the local current density (i) does not exceed the vacancy flux multiplied by Faraday's constant ($j_v \cdot F$), the interface will remain in contact [47]. On the other hand, if i surpasses $j_v \cdot F$, excess vacancies will form and coalesce into pores, thereby raising interfacial resistance and making high rate capability impractical [47]. Operating SSBs under stack pressure and elevated temperatures (e.g., 5 MPa and 60°C) has been effective in improving rate capability by inducing both displacive and diffusional motion of Li atoms [48]; nevertheless, it is considered an auxiliary solution due to the limitations in further increasing stack pressure and temperature [40, 48].

On the other hand, β-phase can inherently introduce an additional driving force for diffusion. Upon stripping, the Li concentration near the interface decreases. If the stripping is limited by the mass transport, it will develop a chemical composition gradient [48]. This gradient can then drive further flux of Li atoms (J_{Li}), which is expressed as follows in the laboratory frame [49]:

$$J_{Li} = -\tilde{D}\nabla c_{Li}(\mathbf{x}), \tag{6}$$

where $\nabla c_{Li}(\mathbf{x})$ is the Li concentration gradient. Here, interdiffusivity $\tilde{D} = X_{Li}D_{Ag} + X_{Ag}D_{Li}$, where $X_{Li\,or\,Ag}$ and $D_{Li\,or\,Ag}$ are the mole fraction and the intrinsic diffusivity of the chemical species in the subscript, respectively. It is thus possible that this flux has contributed to resisting the evolution of morphological instabilities at the MIEC/β-phase along with the flux driven by the vacancy concentration gradient and applied stack pressure. In fact, Krauskopf et al. [48] demonstrated that adding 10 at.% Mg into the Li metal anode can mitigate contact loss at the SE/β-phase interface during discharging, with the consideration of chemical diffusion coefficients. Moreover, it was shown that $Li_7La_{2.75}Ca_{0.25}Zr_{1.75}Nb_{0.25}O_{12}$ garnet exhibits seamless interfacial contact with the Li metal anode when Ag is sputtered on its surface and thus forms Li-Ag alloy upon cycling; the reported interfacial resistance after 150 cycles is also ~7 times lower than the pristine garnet [50]. These findings suggest that additional driving force could indeed help alleviate morphological instabilities to some extent even when solubility in β-phase is limited. Similarly, the presence of alloying elements and the resultant establishment of concentration gradient may have contributed to suppressing morphological instabilities in this SSB.

Upon the removal of Li atoms, the remaining Ag would either stay dissolved in the β-phase or form intermetallic compounds depending on the local composition. Assuming mass-transport-limited stripping, the β-phase will have a concentration profile, where Ag concentration gradually increases and finally reaches the solubility limit (~1 at.% at RT [36, 37]). Interdiffusivity and mechanical properties will vary accordingly. In particular, the interdiffusivity and the mechanical properties of intermetallic compounds can differ greatly from those of the β-phase [51–53]. Nonetheless, provided that the particles of the intermetallic compounds formed are on the nanometer scale in size without agglomeration into microparticles, stripping of Li from these particles would be achieved at an appreciable rate without serious Li depletion near the interface and the resultant increase in interfacial resistance.

The change in alloy composition during stripping affects the alloy's interdiffusivity and mechanical properties (e.g., elastic constants and strength), thereby changing Li transport kinetics [54]. However, its impact is expected not to be significant as long as Ag-rich alloy particles that form upon stripping are distributed uniformly in-plane near the CC side of the MIEC and remain at the nanometer scale in size after stripping. If the CC is perfectly argenphilic, then the equilibrium wetting angle would be zero and the above can be easily achievable. But if it is argenphobic, dewetting and subsequent coarsening could leave big Ag particles at the CC side after Li stripping, which would be very bad for subsequent cycling from both the kinetics and mechanical robustness viewpoints.

5. Design Rules

With the aid of the mechanistic insights above, the rechargeable SSB with the Ag-C nanocomposite anode [25] has

shown outstanding Coulombic efficiency (over 99.8%) and long cycle life (1,000 times). This full-cell performance sheds light on rechargeable SSB development for use as EV batteries, where a cycle life of ≥~5,000 is desirable (a minimum requirement is 800 deep charge-discharge cycles). Here, we discuss various features of an open-porous MIEC interlayer that would help to enhance the cycle life when optimized.

There has not been a detailed analysis of the failure mechanism in this SSB. It is nonetheless expected that the cyclic stress inevitable in the current cell configuration contributes to cell degradation. The maximum thickness of the β-Li_yAg layer is ~25 μm [25], whereas that expected from the areal capacity loading of 6.8 mAh cm^{-2} is ~34 μm. This discrepancy implies that the β-Li_yAg phase is accommodated partially in the porous MIEC interlayer. The plasticity of β-Li_yAg may have allowed it to change shape according to the accessible spaces at a reasonable flow rate. Nevertheless, ~25 μm is still nearly 20% of the full-cell thickness. It has been shown that such volume change can induce the stress amplitude of ~0.4 MPa in LE-based batteries [55]. Since solid components are less effective at relieving mechanical stress than liquid substances, the stress amplitude is likely to be greater in this SSB. Such cyclic stress can cause failure at a stress level lower than a material's static strength [56]. The generated cyclic stress may thus have contributed to limiting the cycle life. This possibility suggests that a carefully structure-designed open-porous MIEC interlayer may outperform the one that consists of randomly packed particles.

Along with the cyclic stresses, charging and discharging rates are one of the cycle life-determining factors. The rate capability examination result of this SSB [25] shows that the achievable cell capacities and specific capacities vary greatly depending on discharging rates. The improvement of the rate capability is thus required to extend the cycle life at a practically reasonable charging/discharging rate. Referring to the aforementioned possible role of Ag transport, it is likely that rate capability is controlled by β-phase's alloy interdiffusivity. The faster the transport is, the more durable the cell would be at a given charging/discharging rate, resulting in the extended cycle life.

As the transport is mediated by interfacial diffusion, the larger the interfacial area and the higher the homologous temperature (i.e., the faster the interdiffusivity [57, 58]), the greater the diffusion flux would be. First, in terms of the interfacial area, the porous structure is favored. The porosity, however, lowers the volumetric capacity and weakens the structural robustness. To enhance the interfacial area at a given porosity, the microstructural architecture and length scales of a porous MIEC interlayer have to be optimized, for instance by introducing more open instead of closed nanopores. Second, in terms of the homologous temperature, metallic elements that have a solubility in Li_{BCC} as well as a solidus temperature that is comparable to or lower than the T_M of Li_{BCC}, such as Mg, are possible candidates. In particular, those that form a eutectic point at the Li-rich region in the phase diagram, similarly to Ag, are likely to be promising; Au and Zn are examples of such elements.

Meanwhile, as the alloy composition varies during cycling, composition-dependent interdiffusivity and mechanical properties and their possible effects on stripping behavior should be investigated. With alloying elements that have limited solubility in Li_{BCC} and form a eutectic point at the Li-rich region, Li stripping behavior would probably be similar to the case of Ag. In contrast, with alloying elements that have greater solubility in Li, the interdiffusivity and mechanical properties of the remaining β-phase could change significantly upon Li stripping. For example, if Mg concentration in Li increases beyond 10 at.%, both displacive deformation and diffusional motion would become less effective as the homologous temperature decreases and the elastic constants/strength increase. It has indeed been shown that submicrometer pores form when cycling Li-Mg alloy and that they cannot be filled in by the external pressure of 15 MPa [48]. Thus, such a system is likely to form another MIEC interlayer constructed of solid-solution alloys, which can function as a 3D framework where β-phase resides [23]. This architecture could be beneficial for garnet-SE-based SSBs, where minimal volume change is desired.

Stack pressure may not be required at all if the structure of an open-porous MIEC interlayer with IEIs is optimized. As discussed briefly in the previous section, it is generally thought that SSBs need stack pressure to avoid interfacial pores and contact losses caused by a large volume change since their solid components lack fluidity. It has been shown that a low stack pressure of ~5 MPa on SSBs can effectively lower the cell impedance and improve cell performance by increasing the interfacial contact area [40]. Higher pressure is, however, known to cause creeping of Li inside the SE and thereby short-circuiting [40]. Meanwhile, if the β-phase is guided to reside in the prereserved porosity of a 3D MIEC interlayer, the degree of a volume change can be greatly reduced. Moreover, if IEIs are decorated on the SE/MIEC interface, they can function as a strong mechanical binder that secures physical contact between SE and MIEC. These components could thus contribute to reducing the magnitude of the required stack pressure and hence lowering the chance of mechanically induced short-circuiting.

6. Outlook

Rechargeable alkali metal SSBs with SEs are an attractive candidate for the next-generation energy storage system. Fueled by the intense interests in them, there has been rapid advancement in SE development, but the overall rechargeable alkali metal SSB technology remains immature. The first task was to improve the bulk ionic conductivity of inorganic SEs, which was impractically low in the early years. This task has been accomplished, taking advantage of computational material genomics [15]. The current computational methods have, however, been a help only to a limited extent regarding interfacial problems, such as instabilities caused by swelling-then-retreating of highly corrosive and mechanically stressful β-phase [2]. In these interfacial issues, kinetic factors of which timescale is not achievable using first-principle calculations are involved, in contrast to the ionic conductivity problem [2]. Examples of such factors are the nucleation and growth of new phases at heterogeneous interfaces, the long-range diffusion of different elements [2], and stress relaxation by diffusional creep (or power-law creep, which

is a hybrid displacive-diffusional process that involves an intermediate level of shear stresses) mechanisms. Furthermore, the evolution of instabilities at the interface itself is considered hard to model due to the nature of the interface that can be summarized as high degrees of structural and chemical freedom.

Nonetheless, it has been recently demonstrated that the deployment of various types of solids altogether for the design of anodes can suppress the electrochemomechanical instabilities [20, 25]. Indeed, the resultant performance of some SSBs has been found to be sufficient for use in consumer electronics, and even vehicular applications (e.g., more than 800 deep charge-discharge cycles). First, a 3D open-porous MIEC architecture is used to host β-phase and enable fast stress relaxation [20, 25, 59, 60]. Second, the use of solid IEI (i.e., an ion-electron insulator) has been proposed as a binder between MIEC and SE to prevent the naked SE/MIEC interface from becoming mechanically unstable due to the deposition of soft β-phase [20] prone to be turning into effectively an adhesion crack. Third, solute elements with a certain degree of solubility in Li_{BCC} were included, thereby enabling Li_{BCC} nucleation inside the MIEC interlayer rather than at the SE/MIEC interface [25], and the asymmetry that develops during battery cycling (attributed to argenphilicity/argenphobicity difference between SE and CC, and mechanical constructions) that reinforce lower R_{ct} and β-phase nucleation barriers on the CC side compared to the SE side. Benefiting from these diverse factors, a long-cycling rechargeable alkali metal SSB has recently been developed [25]. In this cell, β-phase was deposited mostly at the MIEC/CC interface and some inside the porous MIEC, instead of mainly nucleating and growing at the SE/MIEC interface, thereby reducing the pressure on the SE and repressing the evolution of electrochemomechanical instabilities inside the SE [25]. The porous MIEC interlayer can therefore be considered as a buffer and an asymmetric diverter that draws the aggression of the β-phase towards the more ductile and thermochemically stable metallic CC, rather than the fragile and thermochemically unstable ceramic SE. The use of electronically insulating, lithiophobic and argenphobic IEI as a binder between SE and MIEC and the use of lithiophilic and argenphilic CC materials provide driving force for this asymmetry.

Careful examinations of the open-porous MIEC interlayer-based anodes with outstanding full-cell performances provide insights for the further development of rechargeable alkali metal SSBs. First, for the minimization of stress that is exerted on the SEs, the 3D MIEC architectures should have open-porous channels, which can serve as a pipe where β-phase resides. Second, the β-phase deposition at the MIEC/CC interface when the inner surface of the MIEC is decorated with metal nanoparticles suggests that the modification of R_{ct} can manipulate where large quantities of β-phase are first deposited that act as coarsening centers and prevent or delay nucleation/growth at the MIEC/SE side. Third, for the optimization of the rate capability, the composition of metal nanoparticles should be modified so that the resulting alloys have low eutectic melting points. This modification would enable constituting elements to diffuse along the solid interfaces at a rate relevant for industrial applications (e.g., EV), matching the expected areal current density. Finally, the use of IEIs at the SE/MIEC interface would improve mechanical stability, and tuning lithiophilicity/argenphilicity gradient would help establish the asymmetry. These design strategies are expected to further enhance SSB performance, especially in terms of cycle life and rate capability. They also provide opportunities for the development of Na or other alkali metal batteries.

The optimal design of such composite anodes is, however, challenging due to their multidimensional material space and complex temperature-pressure-chemistry window viable for composite processing. Even when only 10 candidates for each solid category are considered, the number of possible combinations already reaches 10^3. Moreover, as metals with low melting points will be deployed inside an MIEC and the MIEC will have an open-porous 3D structure, there are not many methods available for the decoration of IEIs, which are mostly ceramics that require high temperature and pressure for sintering. The spray pyrolysis method [61] is one of the most promising methods that do not apply high temperature and pressure. However, the precursors adopted for this method often react with other solid components that constitute an interlayer. Therefore, thorough understandings of the mechanisms underlying the synergistic effect of combining different classes of materials (M, SE, MIEC, and IEI) and a broader material approach that includes processing and mechanics considerations should be established to narrow down the candidates for each category of materials. Furthermore, the simultaneous development of experimental processing techniques for such composites should be investigated.

Conflicts of Interest

The authors declare that there is no conflict of interest regarding the publication of this article.

Authors' Contributions

S.Y.K and J.L conceived and wrote the manuscript.

Acknowledgments

This work is financially supported by the Samsung Advanced Institute of Technology. S.Y.K gratefully acknowledges partial financial support by the Kwanjeong Scholarship.

Supplementary Materials

The activity coefficient of Ag in β-Li_yAg at infinite dilution (γ^{∞}_{Ag}) was estimated using the CALculation of PHAse Diagrams (CALPHAD) technique in conjunction with Thermo-Calc software. TCAL6 databases for Al-based alloys were used as they include temperature and composition-dependent interaction parameters for the Li-Ag binary pair. γ^{∞}_{Ag} at 150 °C is used instead of that at room temperature as the databases were constructed based on the experimental data points [1] obtained at temperatures near or above

150°C [2]. At this temperature, the calculated chemical activity (Figure S1) is in good accordance with the experimental phase diagram (Figure S2) [3] in the Li-rich region ($X_{Li} > 0.8$), which is the region of interest. We assume that $\gamma^{\infty}_{Ag}(T = 150°C) \sim \gamma^{\infty}_{Ag}(T = 25°C)$ as the temperature derivative of $\ln(\gamma^{\infty}_{Ag})$ is equivalent to $-H^{ex}_{Ag}/RT^2$, [4] which is nearly zero at infinite dilution. Here, H^{ex}_{Ag} is the excess mixing enthalpy, R is the gas constant, and T is the temperature. γ^{∞}_{Ag} can then be estimated from the slope of activity versus composition relation at infinite dilution; thus, $\gamma^{\infty}_{Ag} = 0.00143$. Figure S1: activity of Ag versus the bulk concentration of Li for the Li-Ag binary system. Figure S2: experimentally determined phase diagram of the Li-Ag binary system. Reproduced from Ref. [3]. *(Supplementary Materials)*

References

[1] Q. Zhao, S. Stalin, C. Z. Zhao, and L. A. Archer, "Designing solid-state electrolytes for safe, energy-dense batteries," *Nature Reviews Materials*, vol. 5, no. 3, pp. 229–252, 2020.

[2] Y. Xiao, Y. Wang, S. H. Bo, J. C. Kim, L. J. Miara, and G. Ceder, "Understanding interface stability in solid-state batteries," *Nature Reviews Materials*, vol. 5, no. 2, pp. 105–126, 2020.

[3] P. Sun, R. Bisschop, H. Niu, and X. Huang, *A review of battery fires in electric vehicles*, vol. 56, no. 4, 2020Springer US, 2020.

[4] X. Feng, M. Ouyang, X. Liu, L. Lu, Y. Xia, and X. He, "Thermal runaway mechanism of lithium ion battery for electric vehicles: a review," *Energy Storage Materials*, vol. 10, pp. 246–267, 2018.

[5] J. Zheng, G. Tan, P. Shan et al., "Understanding thermodynamic and kinetic contributions in expanding the stability window of aqueous electrolytes," *Chem*, vol. 4, no. 12, pp. 2872–2882, 2018.

[6] K. Leung, "First-principles modeling of Mn(II) migration above and dissolution from $Li_xMn_2O_4$ (001) surfaces," *Chemistry of Materials*, vol. 29, pp. 2550–2562, 2016.

[7] J. Scheers, S. Fantini, and P. Johansson, "A review of electrolytes for lithium-sulphur batteries," *Journal of Power Sources*, vol. 255, pp. 204–218, 2014.

[8] J. C. Bachman, S. Muy, A. Grimaud et al., "Inorganic solid-state electrolytes for lithium batteries: mechanisms and properties governing ion conduction," *Chemical Reviews*, vol. 116, pp. 140–162, 2015.

[9] A. Manthiram, X. Yu, and S. Wang, "Lithium battery chemistries enabled by solid-state electrolytes," *Nature Reviews Materials*, vol. 2, no. 4, pp. 1–16, 2017.

[10] J. Li, C. Ma, M. Chi, C. Liang, and N. J. Dudney, "Solid electrolyte: the key for high-voltage lithium batteries," *Advanced Energy Materials*, vol. 5, no. 4, pp. 1–6, 2015.

[11] C. Monroe and J. Newman, "The impact of elastic deformation on deposition kinetics at lithium/polymer interfaces," *Journal of the Electrochemical Society*, vol. 152, no. 2, p. A396, 2005.

[12] L. Porz, T. Swamy, B. W. Sheldon et al., "Mechanism of lithium metal penetration through inorganic solid electrolytes," *Advanced Energy Materials*, vol. 7, no. 20, p. 1701003, 2017.

[13] Y. Kato, S. Hori, T. Saito et al., "High-power all-solid-state batteries using sulfide superionic conductors," *Nature Energy*, vol. 1, no. 4, pp. 1–7, 2016.

[14] X. He, Y. Zhu, and Y. Mo, "Origin of fast ion diffusion in super-ionic conductors," *Nature Communications*, vol. 8, no. 1, pp. 1–7, 2017.

[15] Y. Wang, W. D. Richards, S. P. Ong et al., "Design principles for solid-state lithium superionic conductors," *Nature Materials*, vol. 14, no. 10, pp. 1026–1031, 2015.

[16] Y. Zhu, X. He, and Y. Mo, "Origin of outstanding stability in the lithium solid electrolyte materials: insights from thermodynamic analyses based on first-principles calculations," *ACS Applied Materials & Interfaces*, vol. 7, no. 42, pp. 23685–23693, 2015.

[17] Y. Zhu, X. He, and Y. Mo, "First principles study on electrochemical and chemical stability of solid electrolyte-electrode interfaces in all-solid-state Li-ion batteries," *Journal of Materials Chemistry A*, vol. 4, no. 9, pp. 3253–3266, 2016.

[18] W. D. Richards, L. J. Miara, Y. Wang, J. C. Kim, and G. Ceder, "Interface stability in solid-state batteries," *Chemistry of Materials*, vol. 28, no. 1, pp. 266–273, 2016.

[19] Y. Yang, A. Kushima, W. Han, H. Xin, and J. Li, "Liquid-like, self-healing aluminum oxide during deformation at room temperature," *Nano Letters*, vol. 18, no. 4, pp. 2492–2497, 2018.

[20] Y. Chen, Z. Wang, X. Li et al., "Li metal deposition and stripping in a solid-state battery via Coble creep," *Nature*, vol. 578, no. 7794, pp. 251–255, 2020.

[21] D. A. Porter and K. E. Easterling, *Phase Transformations in Metals and Alloys*, CRC press, 2009.

[22] S. Xu, D. W. McOwen, C. Wang et al., "Three-dimensional, solid-state mixed electron-ion conductive framework for lithium metal anode," *Nano Letters*, vol. 18, no. 6, pp. 3926–3933, 2018.

[23] C. Yang, H. Xie, W. Ping et al., "An electron/ion dual-conductive alloy framework for high-rate and high-capacity solid-state lithium-metal batteries," *Advanced Materials*, vol. 31, pp. 1–7, 2018.

[24] Z. Zhu, L. L. Lu, Y. Yin, J. Shao, B. Shen, and H. Bin Yao, "High rate and stable solid-state lithium metal batteries enabled by electronic and ionic mixed conducting network interlayers," *ACS Applied Materials & Interfaces*, vol. 11, no. 18, pp. 16578–16585, 2019.

[25] Y. Lee, S. Fujiki, C. Jung et al., "High-energy long-cycling all-solid-state lithium metal batteries enabled by silver-carbon composite anodes," *Nature Energy*, vol. 5, no. 4, pp. 299–308, 2020.

[26] Z. Wang, X. Li, Y. Chen et al., "Creep-enabled 3D solid-state lithium-metal battery," *Chem*, vol. 6, no. 11, pp. 2878–2892, 2020.

[27] W. Xue, T. Chen, Z. Ren et al., "Molar-volume asymmetry enabled low-frequency mechanical energy harvesting in electrochemical cells," *Applied Energy*, vol. 273, p. 115230, 2020.

[28] S. Kim, S. J. Choi, K. Zhao et al., "Electrochemically driven mechanical energy harvesting," *Nature communications*, vol. 7, 2016.

[29] M. F. Ashby, "Ein erster bericht uber eine darstellung der verformungs-mechanismen in einer art landkarte," *Acta Metallurgica*, vol. 20, no. 7, pp. 887–897, 1972.

[30] J. Duan, Y. Zheng, W. Luo et al., "Is graphite lithiophobic or lithiophilic?," *National Science Review*, vol. 7, no. 7, pp. 1208–1217, 2020.

[31] S. Nanda, A. Gupta, and A. Manthiram, "Anode-free full cells: a pathway to high-energy density lithium-metal batteries," *Advanced Energy Materials*, vol. 11, pp. 1–18, 2021.

[32] S. Randau, D. A. Weber, O. Kötz et al., "Benchmarking the performance of all-solid-state lithium batteries," *Nature Energy*, vol. 5, no. 3, pp. 259–270, 2020.

[33] X. Yang, J. Luo, and X. Sun, "Towards high-performance solid-state Li-S batteries: from fundamental understanding to engineering design," *Chemical Society Reviews*, vol. 49, no. 7, pp. 2140–2195, 2020.

[34] N. Ohta, K. Takada, L. Zhang, R. Ma, M. Osada, and T. Sasaki, "Enhancement of the high-rate capability of solid-state lithium batteries by nanoscale interfacial modification," *Advanced Materials*, vol. 18, no. 17, pp. 2226–2229, 2006.

[35] Z. Wang, L. Yang, J. Liu et al., "Tuning rate-limiting factors to achieve ultrahigh-rate solid-state sodium-ion batteries," *ACS Applied Materials & Interfaces*, vol. 12, no. 43, pp. 48677–48683, 2020.

[36] A. D. Pelton, "The Ag–Li (silver-lithium) system," *Bulletin of Alloy phase diagrams*, vol. 7, no. 3, pp. 223–228, 1986.

[37] V. V. Pavlyuk, G. S. Dmytriv, I. I. Tarasiuk, I. V. Chumak, H. Pauly, and H. Ehrenberg, "Polymorphism of LiAg," *Solid State Sciences*, vol. 12, no. 2, pp. 274–280, 2010.

[38] K. Yan, Z. Lu, H. W. Lee et al., "Selective deposition and stable encapsulation of lithium through heterogeneous seeded growth," *Nature Energy*, vol. 1, 2016.

[39] C. H. P. Lupis, *Chemical thermodynamics of materials*, Elsevier Science Publishing Company, Inc, 1983.

[40] J. M. Doux, H. Nguyen, D. H. S. Tan et al., "Stack pressure considerations for room-temperature all-solid-state lithium metal batteries," vol. 10, pp. 1–6, 2019.

[41] J. Sun, L. He, Y.-C. Lo et al., "Liquid-like pseudoelasticity of sub-10-nm crystalline silver particles," *Nature Materials*, vol. 13, no. 11, pp. 1007–1012, 2014.

[42] Y. Mishin, M. Asta, and J. Li, "Atomistic modeling of interfaces and their impact on microstructure and properties," *Acta Materialia*, vol. 58, no. 4, pp. 1117–1151, 2010.

[43] L. Pauling, "Atomic radii and interatomic distances in metals," *Journal of the American Chemical Society*, vol. 69, no. 3, pp. 542–553, 1947.

[44] H. S. Oh, S. J. Kim, K. Odbadrakh et al., "Engineering atomic-level complexity in high-entropy and complex concentrated alloys," *Nature Communications*, vol. 10, no. 1, pp. 2090–2098, 2019.

[45] S. Bhagat, H. Han, and T. L. Alford, "Tungsten-titanium diffusion barriers for silver metallization," *Thin Solid Films*, vol. 515, no. 4, pp. 1998–2002, 2006.

[46] E. Friedland, N. G. Van Der Berg, J. B. Malherbe et al., "Investigation of silver and iodine transport through silicon carbide layers prepared for nuclear fuel element cladding," *Journal of Nuclear Materials*, vol. 410, no. 1-3, pp. 24–31, 2011.

[47] T. Krauskopf, H. Hartmann, W. G. Zeier, and J. Janek, "Toward a fundamental understanding of the lithium metal anode in solid-state batteries-an electrochemo-mechanical study on the garnet-type solid electrolyte Li 6.25 Al 0.25 La 3 Zr 2 O 12," *ACS applied materials & interfaces*, vol. 11, pp. 14463–14477, 2019.

[48] T. Krauskopf, B. Mogwitz, C. Rosenbach, W. G. Zeier, and J. Janek, "Diffusion limitation of lithium metal and Li–Mg alloy anodes on LLZO type solid electrolytes as a function of temperature and pressure," *Advanced Energy Materials*, vol. 9, 2019.

[49] R. W. Balluffi, S. M. Allen, and W. C. Carter, *Kinetics of Materials*, John Wiley & Sons, 2005.

[50] W. Feng, X. Dong, P. Li, Y. Wang, and Y. Xia, "Interfacial modification of Li/garnet electrolyte by a lithiophilic and breathing interlayer," *Journal of Power Sources*, vol. 419, pp. 91–98, 2019.

[51] K. Li, H. Xie, J. Liu, Z. Ma, Y. Zhou, and D. Xue, "From chemistry to mechanics: bulk modulus evolution of Li-Si and Li-Sn alloys via the metallic electronegativity scale," *Physical Chemistry Chemical Physics*, vol. 15, no. 40, pp. 17658–17663, 2013.

[52] Y. Qi, L. G. Hector, C. James, and K. J. Kim, "Lithium concentration dependent elastic properties of battery electrode materials from first principles calculations," *Journal of the Electrochemical Society*, vol. 161, no. 11, pp. F3010–F3018, 2014.

[53] P. Zhang, Z. Ma, W. Jiang, Y. Wang, Y. Pan, and C. Lu, "Mechanical properties of Li-Sn alloys for Li-ion battery anodes: a first-principles perspective," *AIP Advances*, vol. 6, 2016.

[54] J. Trivisonno and C. S. Smith, "Elastische konstanten von lithium-magnesium legierungen," *Acta Metallurgica*, vol. 9, no. 12, pp. 1064–1071, 1961.

[55] A. J. Louli, M. Genovese, R. Weber, S. G. Hames, E. R. Logan, and J. R. Dahn, "Exploring the impact of mechanical pressure on the performance of anode-free lithium metal cells," *Journal of The Electrochemical Society*, vol. 166, no. 8, pp. A1291–A1299, 2016.

[56] S. Suresh, *Fatigue of Materials*, Cambridge university press, 2012.

[57] C. Zhang, F. Zhang, K. Jin et al., "Understanding of the elemental diffusion behavior in concentrated solid solution alloys," *Journal of Phase Equilibria and Diffusion*, vol. 38, no. 4, pp. 434–444, 2017.

[58] K. Jin, C. Zhang, F. Zhang, and H. Bei, "Influence of compositional complexity on interdiffusion in Ni-containing concentrated solid-solution alloys," *Materials Research Letters*, vol. 6, no. 5, pp. 293–299, 2018.

[59] C. Jin, O. Sheng, J. Luo et al., "3D lithium metal embedded within lithiophilic porous matrix for stable lithium metal batteries," *Nano Energy*, vol. 37, pp. 177–186, 2017.

[60] J. Zhao, G. Zhou, K. Yan et al., "Air-stable and freestanding lithium alloy/graphene foil as an alternative to lithium metal anodes," *Nature Nanotechnology*, vol. 12, no. 10, pp. 993–999, 2017.

[61] T. Ryll, P. Reibisch, L. Schlagenhauf et al., "Lanthanum nickelate thin films deposited by spray pyrolysis: crystallization, microstructure and electrochemical properties," *Journal of the European Ceramic Society*, vol. 32, no. 8, pp. 1701–1709, 2012.